Human Induced Pluripotent Stem Cells Differentiate Into Functional Mesenchymal Stem Cells and Repair Bone Defects

DMITRIY SHEYN,[a,b] SHIRAN BEN-DAVID,[a,b] GALINA SHAPIRO,[c] SANDRA DE MEL,[a,b] MAXIM BEZ,[a,b,c] LOREN ORNELAS,[b,d] ANAIS SAHABIAN,[b,d] DHRUV SAREEN,[c,d,e] XIAOYU DA,[f] GADI PELLED,[a,b,c] WAFA TAWACKOLI,[a,b,e,f] ZHENQIU LIU,[g] DAN GAZIT,[a,b,c,f] ZULMA GAZIT[a,b,c]

Key Words. Human induced pluripotent stem cells • Transforming growth factor-β • Mesenchymal stem cells • Bone regeneration

[a]Department of Surgery,
[b]Board of Governors
Regenerative Medicine
Institute, [d]iPSC Core Facility,
The David and Janet Polak
Stem Cell Laboratory,
[e]Department of Biomedical
Sciences, [f]Biomedical Imaging
Research Institute, and
[g]Biostatistics and
Bioinformatics Core, Samuel
Oschin Comprehensive
Cancer Institute, Cedars-Sinai
Medical Center, Los Angeles,
California, USA; [c]Skeletal
Biotech Laboratory, Hebrew
University of Jerusalem,
Jerusalem, Israel

Correspondence: Zulma Gazit,
Ph.D., Department of Surgery and
Cedars-Sinai Regenerative
Medicine Institute, Cedars-Sinai
Medical Center, 8700 Beverly
Boulevard, Los Angeles, California
90048, USA. Telephone: 310-248-
8562; E-Mail: zulma.gazit@csmc.
edu

ABSTRACT

Mesenchymal stem cells (MSCs) are currently the most established cells for skeletal tissue engineering and regeneration; however, their availability and capability of self-renewal are limited. Recent discoveries of somatic cell reprogramming may be used to overcome these challenges. We hypothesized that induced pluripotent stem cells (iPSCs) that were differentiated into MSCs could be used for bone regeneration. Short-term exposure of embryoid bodies to transforming growth factor-β was used to direct iPSCs toward MSC differentiation. During this process, two types of iPSC-derived MSCs (iMSCs) were identified: early (aiMSCs) and late (tiMSCs) outgrowing cells. The transition of iPSCs toward MSCs was documented using MSC marker flow cytometry. Both types of iMSCs differentiated in vitro in response to osteogenic or adipogenic supplements. The results of quantitative assays showed that both cell types retained their multidifferentiation potential, although aiMSCs demonstrated higher osteogenic potential than tiMSCs and bone marrow-derived MSCs (BM-MSCs). Ectopic injections of *BMP6*-overexpressing tiMSCs produced no or limited bone formation, whereas similar injections of *BMP6*-overexpressing aiMSCs resulted in substantial bone formation. Upon orthotopic injection into radial defects, all three cell types regenerated bone and contributed to defect repair. In conclusion, MSCs can be derived from iPSCs and exhibit self-renewal without tumorigenic ability. Compared with BM-MSCs, aiMSCs acquire more of a stem cell phenotype, whereas tiMSCs acquire more of a differentiated osteoblast phenotype, which aids bone regeneration but does not allow the cells to induce ectopic bone formation (even when triggered by bone morphogenetic proteins), unless in an orthotopic site of bone fracture. STEM CELLS TRANSLATIONAL MEDICINE *2016;5:1447–1460*

SIGNIFICANCE

Mesenchymal stem cells (MSCs) are currently the most established cells for skeletal tissue engineering and regeneration of various skeletal conditions; however, availability of autologous MSCs is very limited. This study demonstrates a new method to differentiate human fibroblast-derived induced pluripotent stem cells (iPSCs) to cells with MSC properties, which we comprehensively characterized including differentiation potential and transcriptomic analysis. We showed that these iPS-derived MSCs are able to regenerate nonunion bone defects in mice more efficiently than bone marrow-derived human MSCs when overexpressing *BMP6* using a nonviral transfection method.

INTRODUCTION

Mesenchymal stem cells (MSCs) are currently the most established cells for skeletal tissue engineering and regeneration of various skeletal conditions. The embryonic origin of MSCs remains unclear, although some studies indicate a possible origin for MSCs in a supporting layer of the dorsal aorta in the aorta-gonad-mesonephros region [1, 2]. Consistent with these findings, MSC-like cells have been found circulating in fetal human blood [3]. In adult humans, MSCs appear to be resident in many tissues, functioning in normal tissue turnover. MSCs have been isolated from various adult tissues, including bone marrow and adipose tissue. These cells have been shown to differentiate successfully into osteogenic, chondrogenic, and adipogenic lineages in vitro [4–6]. When tissue repair is required, MSCs can be stimulated to proliferate and differentiate. When genetically modified, these multipotent cells have been shown to form and regenerate

bone in vivo in multiple animal models, providing a gene- and cell-mediated therapeutic platform for multiple potential clinical orthopedic applications [7–11]. Although the frequency of autologous MSCs with aging does not change much [12, 13], unfortunately self-renewal ability and functionality in tissue regeneration of these cells is impaired [13].

The prevalence of musculoskeletal disorders in older populations, together with the challenge of an aging world population, has motivated researchers to investigate the impact of aging on the regenerative properties of MSCs, given their potential as an autologous treatment [14]. Although conflicting results exist, in a variety of organs the regenerative potential of MSCs appears to decline with age [15–17]. Therefore, there is a need for an alternative inexhaustible source of MSCs to treat skeletal disorders. Recently discovered induced pluripotent stem cells (iPSCs) [18] provide a feasible solution to this problem.

Human embryonic stem cells (ESCs) are capable of inducing mesenchymal tissue formation in vivo [19, 20]. Although ESCs were believed to be immunoprivileged, they have been shown to possess immunogenicity after differentiation [21]. In addition, many ethical questions and debates have arisen from the use of ESCs [22], whereas the use of autologous iPSCs poses no ethical dilemmas. By overcoming the immunologic and ethical problems associated with ESCs, the use of iPSCs opens a new avenue for cell transplantation-based regenerative medicine [23]. Thus iPSCs, which are aged cells that possess properties of young/ embryonic cells, could solve one of the bottlenecks for clinical cell therapy, which is the shortage of functional autologous MSCs. iPSCs have been shown to be able to differentiate into skeletal muscle [24, 25], contribute to cardiovascular repair [26, 27], and induce adipogenic differentiation in vitro [23]. Gene-modified cell therapy has been established for bone [11] and other target tissues [28]. Recently, Levi et al. showed that iPSCs can be directed toward osteogenic differentiation in the presence of bone morphogenetic protein 2 (BMP2) [29]. In that study, no teratoma formation was observed, despite the fact that no differentiation of iPSCs was induced before implantation. However, tumorigenicity of pluripotent stem cells is still an open question [30], and it is less likely that iPSCs will be used in the clinical setting unless there is a well-controlled differentiation procedure that rules out any chance of tumor formation.

The transforming growth factor (TGF)-β family has more than 30 members, including TGF-β-s, activins, nodal, BMPs, and growth differentiation factors. These multifunctional cytokines are involved in the morphogenesis of many organs as well as in the homeostasis of adult tissues [31, 32]. Interestingly, TGF-β has been found to be involved not only in suppressing iPSC generation [33], but also in maintaining pluripotency in iPSCs [32, 34]. On the one hand, inhibition of TGF-β in iPSCs was shown to drive the cells toward the MSC-like phenotype [35]; on the other hand, treatment of cells with TGF-β along with other factors reprogrammed the cells toward the osteogenic lineage [36, 37].

The BMP family and its 20 identified members play an important role in osteogenesis [38, 39]. We previously showed that MSCs that have been genetically modified to overexpress a *BMP* gene can regenerate bone defects and induce bone formation in vivo without the need for massive quantities of BMP protein or harvested bone grafts [7–10, 40, 41]. To date, a number of studies have been conducted to determine the most suitable BMP for osteogenic differentiation in vitro and in vivo. Most of these studies have been conducted with the aid of viral gene delivery

[38, 42–47]. Experiments involving MSCs infected with adenoviruses carrying 14 different human isoforms of BMP revealed that *BMP2*, *BMP6*, and *BMP9* are the most potent inducers of osteoblast differentiation in MSCs [43, 47]. We previously showed that *BMP2* gene overexpression in MSCs induces bone formation and heals bone defects in vivo [10, 41, 48–50]. Although less popular, *BMP6* is another prominent candidate for use in bone regeneration. Our studies have shown that nonviral genetic engineering of bone marrow-derived MSCs (BM-MSCs) [48, 51] and adipose–derived stem cells [8, 51, 52] with *BMP6*-encoding plasmid DNA leads to potent bone formation in vivo [8, 9, 52]. In the present study, overexpression of *BMP6* was induced in iMSCs and BM-MSCs to aid ectopic bone formation. BM-MSCs were used as the gold standard for bone stem cell therapy. We developed a new reproducible method to differentiate iPSCs into cells that possess MSC characteristics (iMSCs) and discovered two separate cell populations with different morphologies and expression profiles, separated based on the timing of their outgrowth from embryoid bodies (EBs). We hypothesized that these cells would differ in MSC characteristics and potential for bone formation. To pursue this hypothesis, we characterized the cells, evaluated their bone formation capacities in both ectopic and radial segmental defect models, and compared them to BM-MSCs.

MATERIALS AND METHODS

Human iPSC Generation

Healthy control dermal fibroblasts were obtained from the Coriell Institute for Medical Research (Camden, NJ, https://www.coriell.org) or derived from healthy donors at Cedars-Sinai Medical Center. Reprogramming of the lines was performed using plasmid vectors (Addgene, Cambridge, MA, http://www.addgene.org), adapted from a previously published protocol [53–55]. Briefly, a Human Dermal Fibroblast Nucleofection Kit (Lonza, Portsmouth, NH, http://www.lonza.com) was used to make the virus-free iPSC lines. Briefly, fibroblasts (0.8 $\times$ 10^6 cells per nucleofection) were harvested and centrifuged at 200g for 5 minutes. The cell pellet was resuspended carefully in Nucleofector Solution (VPD-1001; Lonza) and combined with the episomal plasmid expression of six factors—*OCT4*, *SOX2*, *KLF4*, *L-MYC*, *LIN28*, and *p53* shRNA—by plasmid nucleofection. This method has a significant advantage over viral transduction, because the genes do not integrate and are instead expressed episomally in a transient fashion. The cell/DNA suspension was transferred into the Nucleofection solution (Lonza), and a fibroblast-specific program was applied. All cultures were maintained under normal oxygen conditions (5% O$_2$) during reprogramming, which further enhanced the efficiency of iPSC generation. The culture medium was maintained for 48 hours and gradually changed to human iPSC (hiPSC) medium containing small molecules to enhance reprogramming efficiency. These small molecules included the following: (a) sodium butyrate; (b) a glycogen synthase kinase 3β inhibitor of the Wnt/β-catenin signaling pathway (CHIR99021, EMD Millipore, Billerica, MA, http://www.emdmillipore.com); (c) a mitogen-activated protein kinase pathway inhibitor; and (d) a selective inhibitor of TGF-β type I receptor ALK5 kinase, type I activin/nodal receptor ALK4, and type I nodal receptor ALK7. Colonies with an embryonic stem/iPSC-like morphology appeared 25 to 31 days later. Subsequently, colonies with the best morphology were picked and transferred to layers of a standard hiPSC medium and Matrigel matrix (BD Biosciences, San Jose, CA, http://www.

bdbiosciences.com) for feeder-independent maintenance of hiPSCs in chemically defined mTeSR1 medium (Stemcell Technologies, Vancouver, BC, Canada, http://www.stemcell.com). Independent iPSC clones were picked from each reprogrammed fibroblast sample, further expanded, and cryopreserved. The iPS phenotype was established and characterized in previous publications [54–56].

BM-MSC Isolation

Fresh human bone marrow samples were purchased from Lonza, and human BM-MSCs were isolated according to a standard procedure [48]. Briefly, bone marrow was washed with phosphate-buffered saline (PBS) and centrifuged at $900g$ for 10 minutes. The pellet was resuspended in PBS, after which it was layered on lymphocyte separation medium (Valeant Pharmaceuticals International, Laval, QC, Canada, http://www.valeant.com) and centrifuged at $900g$ for 30 minutes at 25°C without a break. Mononuclear cells were collected and plated at a density of 2×10^5 cells per cm^2. Media were changed twice per week.

iMSC Derivation

To reprogram iPSCs into iMSCs, iPSCs were dissociated with the aid of Versene EDTA (Thermo Fisher Scientific Life Sciences, Waltham, MA, http://www.thermofisher.com) and seeded into nonadherent 384-well conical polymerase chain reaction plates, 10,000 cells per well, with Iscove's modified Dulbecco's medium (IMDM) (MDM basal media, 17% KnockOut Serum Replacement, 1% minimal essential medium nonessential amino acids, 110 mM 2-mercaptoethanol, and 1% PSA antifungal-antibacterial solution [Thermo Fisher Scientific Life Sciences]). On day 2, the EBs were transferred to nonadherent 2.4-μg/cm^2 poly-HEMA-coated flasks and cultured for 3 more days. On day 5, the EBs were transferred to 1% gelatin-treated flasks for 3 more days of culture. On day 8, some EBs attached to the surface and cells grew outward from the EBs. The nonattached EBs were transferred to another 1% gelatin-coated flask. During this process (Fig. 1A), two populations were identified: cells that migrated out of the EB during days 2–5 (attached cells) and cells that grew out of the EB during days 5–8, after the EB had been transferred to another plate (transferred cells). Both cell types were fed with medium supplemented with 10 ng/ml TGF-β1 (R&D Systems, Minneapolis, MN, http://www.rndsystems.com) on days 8–10, after which the medium was switched to standard DMEM culture medium containing 10% fetal bovine serum, 2 mM L-glutamine, and 100 U/ml penicillin/streptomycin (Thermo Fisher Scientific Life Sciences). The medium was changed twice a week, and the cells were split upon confluence in a 1:3 ratio. The same protocol of iMSC derivation was performed using three different iPSC control lines.

MSC Marker Expression: Flow Cytometry

The transition of cells toward the MSC stage was monitored using flow cytometry of MSC surface markers CD105, CD90, and CD44. Adherent cells were cultured until confluence had been reached, and MSC surface marker expression was analyzed longitudinally up to passage 6. At a confluence of 70%, the cells were detached using trypsin-EDTA, washed with phosphate-buffered saline (PBS), and resuspended in fluorescence-activated cell sorting buffer consisting of 2% bovine serum albumin and 0.1% sodium azide in PBS. The cells were stained with mouse antihuman CD90-FITC (BD Biosciences), mouse antihuman CD29-PB (Exbio

Antibodies, Vetec, Czech Republic, http://www.exbio.cz), and antihuman CD105-PE (Ancell Corp., Stillwater, MN, http://www.ancell.com), and bonded primary antibodies were detected using the following isotypes: mouse IgG2a-FITC (Miltenyi Biotec, Cambridge, MA, http://www.miltenyibiotec.com), mouse IgG1-PB (AbD Serotec, Raleigh, NC, http://www.abdserotec.com), and mouse IgG1-PE (BD Biosciences), respectively. Cells were analyzed for expression of the antigens using an LSRFortessa cell analyzer (BD, Heidelberg, Germany, http://www.bd.com/de/) and BD Diva software version 6.1.3 for data collection. Gating was done to include all live cells. Nonspecific fluorescence was detected using isotypes alone and subtracted from the experiment's detection values. The analysis was repeated separately using three different cell types: attached iMSCs (aiMSCs), transferred iMSCs (tiMSCs), and BM-MSCs.

In vitro cell proliferation was assessed using cell counts and the trypan blue exclusion test. Cells were seeded at a density of 5×10^3 cells per cm^2, then grown for 4–6 days, trypsinized, and counted using the Countess automated cell counter (Thermo Fisher Scientific Life Sciences). The cells were reseeded at the above density and labeled as passage 2. This process was repeated until the cells reached passage 8. The doubling rate was calculated by dividing the counted number of cells per well by 2 times the number of initially seeded cells times the number of days in culture. The result represents the number of doublings per cell per day.

Cell tumorigenic potential was tested by performing a soft agar assay, as previously published [57] and in accord with the protocol provided by the manufacturer (Cytoselect; Cell Biolabs, San Diego, CA, http://www.cellbiolabs.com).

Gene Expression: RNA Sequencing

Correlation With Tissues and Cell Lines

The RNA sequencing-based gene expression profile of BM-MSCs, aiMSCs, and tiMSCs was compared against reference expression profiles downloaded from Medicalgenomics (http://medicalgenomics.org/). Both next-generation sequencing-based expression profiles of 11 cell lines and tissues and microarray-based profiles of 101 cell lines and tissues were used as references. All expression data were preprocessed with quintile normalization, after which pairwise global correlations among cell lines aiMSCs, tiMSCs, BM-MSCs, and others were calculated. To adjust for a multiplicity problem in statistical tests, a small p value (.00001) was used for detecting real correlations among the cell lines.

Functional Gene Analysis

The gene expression profile in both types of iMSCs was studied using RNA sequencing and compared with that of BM-MSCs. Three pairwise comparisons of gene expression were made for the three cell populations. For each comparison, significantly upregulated genes were defined as having a log2(fold change) >2 and a p value <.05, whereas significantly downregulated genes were defined as having a log2(fold change) less than −2 and a p value <.05. Therefore, for each comparison, two lists of significantly differently expressed genes were generated. Each list was ranked from the greatest absolute log2(fold change) to the smallest absolute log2(fold value). Each ranked list was deposited into DAVID software for a comparison against a *Homo sapiens* background [58]. The functional annotation clustering analytic module was used with an enrichment score >1.3 cutoff to define statistically significantly enriched terms for each list [58]. In addition to the default annotation categories, the pathways
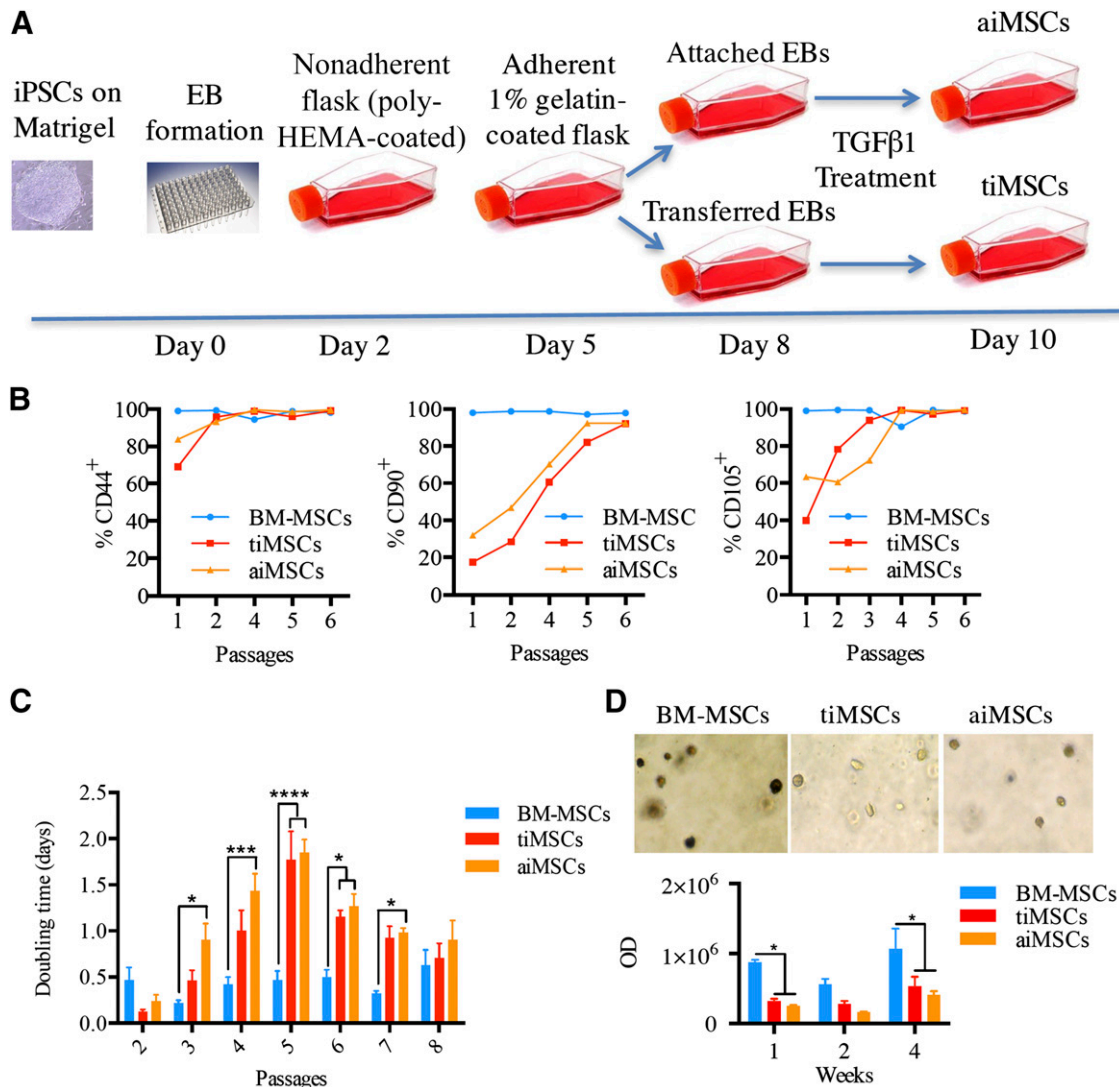
Figure 1. Transformation of iPSCs into iMSCs. **(A):** Schematic differentiation protocol of iPSCs to iMSCs and formation of two different populations: aiMSCs and tiMSCs. **(B):** aiMSCs, tiMSCs, and BM-MSCs at passages 1 through 6 were immunostained for CD105, CD90, and CD44 expression and analyzed using flow cytometry. **(C):** aiMSCs, tiMSCs, and BM-MSCs were counted while passaging to estimate the proliferation rate. **(D):** iMSCs, tiMSCs, and BM-MSCs were grown on soft agar, and their ability to form colonies was evaluated using colorimetric Cytoselect assay for tumorigenicity. Results are presented as means $\pm$ SE. $*, p \leq .05$; $**, p \leq .01$; $***, p \leq .001$; $****, p \leq .0001$. Abbreviations: aiMSC, attached iMSC; BM-MSC, bone marrow-derived MSC; EB, embryoid body; HEMA, hydroxyethyl methacrylate; iMSC, iPSC-derived MSC; iPSC, induced pluripotent stem cell; MSC, mesenchymal stem cell; OD, optical density; TGF, transforming growth factor; tiMSC, transferred iMSC.

and tissue expression categories were selected for analysis, which resulted in a list of enriched terms, pathway enrichment, and tissue expression pattern resemblance for each list. The six lists were combined to create a table reflecting the differences in gene expression between (a) BM-MSCs and tiMSCs and (b) BM-MSCs and aiMSCs.

In Vitro Differentiation

Cultured iMSCs were assayed for their mesenchymal lineage differentiation potential [59]. Adipogenic differentiation was induced by culturing the cells for 2 weeks in adipogenic medium [10, 60], after which differentiation was assessed using Oil Red O stain as an indicator of intracellular lipid accumulation and quantified using spectrophotometry [60].

Chondrogenic differentiation of iMSCs and BM-MSCs was achieved using chondrogenic supplements, as previously described [59, 61, 62]. Briefly, aliquots of 5×10^5 cells were pipetted onto dry 6.5-mm-diameter, 0.4-μm pore size polycarbonate Transwell filters (Corning Life Sciences, Tewksbury, MA, http://www.corning.com/lifesciences) and spun in a 24-well plate (200*g*, 5 minutes). The culture was continued in the 24-well plate, and the medium was replaced every second day for up to 21 days. Chondrogenic differentiation was assessed by measuring the expression of cartilage-specific *Collagen type II*, *Aggrecan*, and *Sox9* marker genes.

Osteogenic differentiation was induced by culturing iMSCs for 1 or 2 weeks in osteogenic medium, after which the cells were quantitatively tested for alkaline phosphatase (ALP) activity and *Collagen type I* gene expression [51, 52, 59].

Nonviral Transfection

The overexpression of the reporter gene *EGFP* or the osteogenic gene *BMP6* was achieved using the pCMV-EGFP-N1 and pCMV-cDNA3-rhBMP-6 plasmids, respectively, with the aid of the Nucleofector device (Amaxa Biosystems, Cologne, Germany, http://www.amaxa.com) and an MSC-specific nucleofection buffer, as reported elsewhere [8, 48, 51, 52]. Immediately after nucleofection, the cells were plated in complete growth medium containing 20% fetal bovine serum; they were then maintained in culture for 24 hours, and nucleofection efficiency was analyzed by flow cytometry for *GFP* expression using an LSR-II FACS (BD Biosciences) and BD Diva software for data collection and analysis. The transfection efficiency was evaluated by determining the percentage of GFP-expressing cells of the total viable cells as well as the mean fluorescence intensity per cell. The efficiency of BMP6 nucleofection was determined by evaluating the secretion of BMP6 into media detected by performing an enzyme-linked immunosorbent assay (ELISA) for BMP6 (R&D Systems) [51, 52].

In Vivo Bone Formation

The Cedars-Sinai Institutional Animal Care and Use Committee approved all procedures described in this study. For in vivo studies, the cells were transfected with *BMP6*, lifted 24 hours later, and prepared for implantation.

Ectopic Model

To evaluate the in vivo osteogenic potential of the cells after nucleofection, we first anesthetized immunodeficient (NOD/SCID) mice by administering 2%–3% isoflurane and placing the animals on a 37°C heating pad. Aliquots of 3×10^6 cells were resuspended in 50 μl fibrin gel (Tisseel kit; Baxter, Vienna, Austria, http://www.baxter.com) and injected into the thigh muscles of the animals (*n* = 5). Each mouse received one injection of MSCs (aiMSCs, tiMSCs, or BMSCs) that had been nucleofected with *BMP6*. Bone formation was evaluated after 4 weeks using microcomputed tomography (μCT). The mice were euthanized, and their limbs were harvested for histologic analysis.

Radial Defect Model

A nonunion radial fracture was created as previously described [50, 63]. Briefly, NOD/SCID female mice (*n* = 7 per group), ages 6–8 weeks, were each anesthetized by an intraperitoneal injection of a ketamine-xylazine mixture, and the skin of the forelimb was swabbed with isopropyl alcohol (70%) and chlorhexidine gluconate (0.5%). The skin was cut, and a 1.5-mm defect in the radius was created. For microscopic cell identification, the cells were trypsinized and labeled with Vibrant-CM-DiI (Thermo Fisher Scientific Life Sciences), as previously described [9]. Aliquots of 10^6 cells were seeded on precut $1 \times 1 \times 1.5$-mm collagen type I biodegradable scaffolds (DuraGen; Integra LifeSciences, Plainsboro, NJ, http://www.integralife.com), and the scaffolds were implanted into the defect site. In control mice, a defect was created, but only an acellular collagen sponge was implanted. Orthotopic bone formation was monitored using in vivo μCT once every 4 weeks for 8 weeks.

Analysis of Bone Formation In Vivo Using μCT

In vivo bone formation was evaluated over time by performing μCT analyses. All μCT procedures used in this study were previously described in detail by Kallai et al. [64]. The mice underwent in vivo μCT scanning while anesthetized 4 weeks after ectopic cell implantation and during day 0, week 4, and week 8 after radial defect creation using a preclinical cone-beam in vivo μCT system (vivaCT 40; Scanco Medical, Brüttisellen, Switzerland, http://www.scanco.ch). Microtomographic slices were acquired using an x-ray tube potential of 55 kVp and reconstructed at a spatial nominal resolution of 35 μm. A constrained three-dimensional (3D) Gaussian filter (σ = 0.8 and support = 1) was used to partly suppress noise found in the volumes. The bone was segmented from bone marrow and soft tissue using a global thresholding procedure [65]. Newly formed bone in the ectopic model was separated from the animal's femur and tibia by manual contouring [66]. Defect margins were located on day 1 scans and aligned to a standard position [64]. Then, newly formed bone (3.15 mm along the length axis) was segmented using a manual contouring procedure and analyzed using 3D histomorphometric evaluation. The following morphometric parameters were evaluated: bone volume density, calculated as the ratio between the bone volume (which represents the volume of mineralized tissue) and the total volume of the volume of interest analyzed; connectivity density (1/mm^3), describing the porosity of the bone sample and showing how branched the bone tissue structure is; average trabecular thickness (mm), calculated as average thickness of all bone voxels and bone mineral density, which is based on standardization of scans of hydroxyapatite samples, determined for newly formed bone on the basis of microtomographic data sets by using direct 3D morphometry [66].

Histologic and Immunofluorescence Analysis

The harvested limbs were fixed in 4% formalin, decalcified using 0.5 M EDTA solution (pH 7.4), dehydrated, and embedded in paraffin. Standard hematoxylin and eosin staining was performed on the paraffin-embedded sections in a manner previously reported [8, 9]. For immunofluorescent staining, tissues were deparaffinized, and the antigens were retrieved by incubation in preheated Target Retrieval Solution (Dako, Carpinteria, CA, http://www.dako.com) for 45 minutes at 37°C. Nonspecific antigens were blocked by applying blocking serum-free solution (Dako). Slides were stained with primary antibodies against human bone sialoprotein (BSP) and osteocalcin (OC) to examine osteogenic differentiation. The primary antibodies were applied to the slides, incubated at 4°C overnight, and washed with PBS; the slides were then incubated with secondary antibodies (supplemental online Table 1) for 1 hour at room temperature, after which they were washed (supplemental online Table 1) with PBS. The slides were stained with 4′,6-diamidino-2-phenylindole dihydrochloride (DAPI, 1 μg/ml) for 5 minutes in the dark, after which they were again washed three times with PBS. VectaMount mounting medium (Vector Laboratories, Burlingame, CA, http://vectorlabs.com) was applied to the tissue. The slides were imaged using a four-channel Laser Scanning Microscope 780 (Zeiss, Pleasanton, CA, http://www.xradia.com) with $\times$20 magnification, z-stacking, and 3×5 tile scanning. For zoomed images, a single z-stacked image was generated using $\times$40 magnification. All samples were scanned using the same gain and exposure settings.

Statistical Analysis

GraphPad Prism 6.0b software (GraphPad, San Diego, CA, http://www.graphpad.com) was used to analyze the data. Results are

presented as means $\pm$ SE. Longitudinal data analysis was conducted using one- or two-way analysis of variance with repeated measures and the Bonferroni posttest. To assess significance, $p <$ .05 was considered statistically significant.

RESULTS

Characterization of iMSC Proliferation and Surface Markers

To monitor the transition of iPSCs to the MSC-like phenotype, a longitudinal study comparing MSC surface marker expression in aiMSCs, tiMSCs, and BM-MSCs at passages 1–6 was done using flow cytometry (Fig. 1B). After a few passages in culture, iMSCs express CD44, CD90, and CD105 similarly to BM-MSCs. Although both aiMSCs and tiMSCs reach 96% CD44$^+$ cells as early as passage 2, they appear to differ in their rate of CD90 and CD105 acquisition. aiMSCs had a consistently greater rate of CD90$^+$ compared with tiMSCs until both reached 94% at passage 6, whereas CD105 was mostly expressed in more of the tiMSCs until passage 4, when all three cell populations were ~96% CD105$^+$.

The proliferation analysis showed that both types of iMSCs have an overall significantly increased proliferation rate compared with BM-MSCs over the first eight passages ($p <$ .01), with no significant difference between aiMSC and tiMSCs overall or at any specific time point ($p >$ .05) (Fig. 1C). aiMSCs and tiMSCs reached a maximum of ~1.8 doublings per day at passage 5 compared with ~0.5 doublings per day for BM-MSCs. The doubling rate decreased after passage 5 for iMSCs, reaching a rate similar to that of BM-MSCs, ~0.8 doublings per day, at passage 8. Given the increased proliferation rate of iMSCs (Fig. 1C), we sought to exclude the presence of residual undifferentiated cells using a soft agar assay that was performed as previously reported [57]. Interestingly, BM-MSCs displayed significantly ($p <$ .05) (Fig. 1D) higher colony formation rates in soft agar than both iMSC types despite having a lower doubling rate. The soft agar assay was performed instead of the teratoma formation assay because of higher accuracy, lower variability, and reduction in animal use.

Gene Expression Profiling

Gene expression was profiled using RNA sequencing and showed that in tiMSCs and aiMSCs, 1,563 and 1,290 genes were significantly up- or downregulated, respectively, compared with BM-MSCs, and that 582 genes were significantly different in their expression between aiMSCs and tiMSCs (Fig. 2A). All three pairwise global correlation coefficients between aiMSCs, tiMSCs, and BM-MSCs were high ($r >$ .92) (Fig. 2B). The strongest correlation found was between aiMSCs and tiMSCs. The gene expression profiles of BM-MSCs, tiMSCs, and aiMSCs were not found to have any significantly similar expression profiles among the 112 tested cell lines and primary tissues ($r <$ .4). The largest correlation found was to the transcriptome of bone and connective tissue, but it was not significant.

Functional gene expression analysis showed that the significantly up- and downregulated genes were involved in many key aspects of the therapeutic potential of iMSCs, such as proliferation, differentiation, and inflammatory response (Fig. 2C). In addition, this analysis also indicated three principal signal transduction pathways: Wnt, TGF-β, and tumor necrosis factor, whose differential expression could mediate the aforementioned differences.

Differentiation Potential

Both types of iMSCs were differentiated in vitro using adipogenic, chondrogenic, or osteogenic supplements, and the extent of cell differentiation was evaluated by performing quantitative assays and gene expression analysis. Adipogenic differentiation in vitro resulted in lipid accumulation in the cells, as evident by Oil Red O staining and the optical density of stained cultures (Fig. 3A). Although all three cell types stained significantly stronger on day 14 compared with day 0 ($p <$ .0001), BM-MSCs had the strongest staining on day 14 compared with tiMSCs ($p >$ .05) but not aiMSCs ($p <$ .05).

After 21 days of chondrogenic differentiation, gene expression analysis of chondrogenic marker genes was performed and normalized to day 0 of the experiment. Although Collagen type II was significantly upregulated in BM-MSCs (10^3-fold, $p <$ .05) compared to other cell types, no significant differences of Aggrecan or Sox9 were found between the three cell types.

The osteogenic response was measured by determining the gene expression of the osteogenic marker genes ALP and Collagen type I and by performing an ALP colorimetric assay. Significant differences between the cell types were found as early as day 7. On day 7, BM-MSCs and tiMSCs expressed significantly higher levels of ALP ($p <$ .001) (Fig. 3C) compared to aiMSCs; however, aiMSCs were found to have significantly higher ALP activity ($p <$ .0001) (Fig. 3D) than other cell types at this time point. On day 14, both tiMSCs and aiMSCs expressed significantly higher levels of Collagen type 1 ($p <$ .01) (Fig. 3C) than BM-MSCs, but aiMSCs were found to have significantly higher ALP activity ($p <$ .0001) (Fig. 3D) than other cell types.

Overall, the results showed that both cell types (aiMSCs and tiMSCs) possess multidifferentiation potential (Fig. 3A–3D). Although no significant differences between the adipogenic and chondrogenic potentials of aiMSCs and tiMSCs were found, aiMSCs displayed a significantly higher osteogenic potential in vitro compared with tiMSCs or BM-MSCs (Fig. 3D).

Transfection Efficiency With Reporter and Therapeutic Genes

To elucidate the potential of the cells to serve as gene therapy and stem cell therapy platforms, we evaluated their ability to be transfected with a reporter and a therapeutic gene and compared them to the gold standard BM-MSCs. First, the cells were nucleofected with the GFP reporter gene using a previously established method [8, 48, 51, 52], and the transfection efficiency was estimated using flow cytometry. Surprisingly, aiMSC and tiMSC nucleofection was significantly ($p <$ .0001) more efficient than BM-MSC nucleofection, resulting in almost 100% GFP-expressing iMSCs compared with almost 90% of BM-MSCs (Fig. 4A), and significantly higher (~fourfold, $p <$ .0001) mean fluorescence intensity, as measured with flow cytometry (Fig. 4B). Although no significant difference was found between aiMSCs and tiMSCs in the percentage of GFP-expressing cells (Fig. 4A), aiMSCs were significantly more fluorescent ($p <$ .0001) (Fig. 4B). Next, we compared the gene expression of a transfected therapeutic gene, BMP6, between the various cell types. BMP6 protein secretion into the media (tested by ELISA) by tiMSCs was found to be significantly higher (threefold; $p <$ .0001) than BM-MSCs and higher than aiMSCs (1.25 fold; $p <$ .0001), which also secreted significantly more BMP6 than BM-MSCs (twofold; $p <$ .0001).
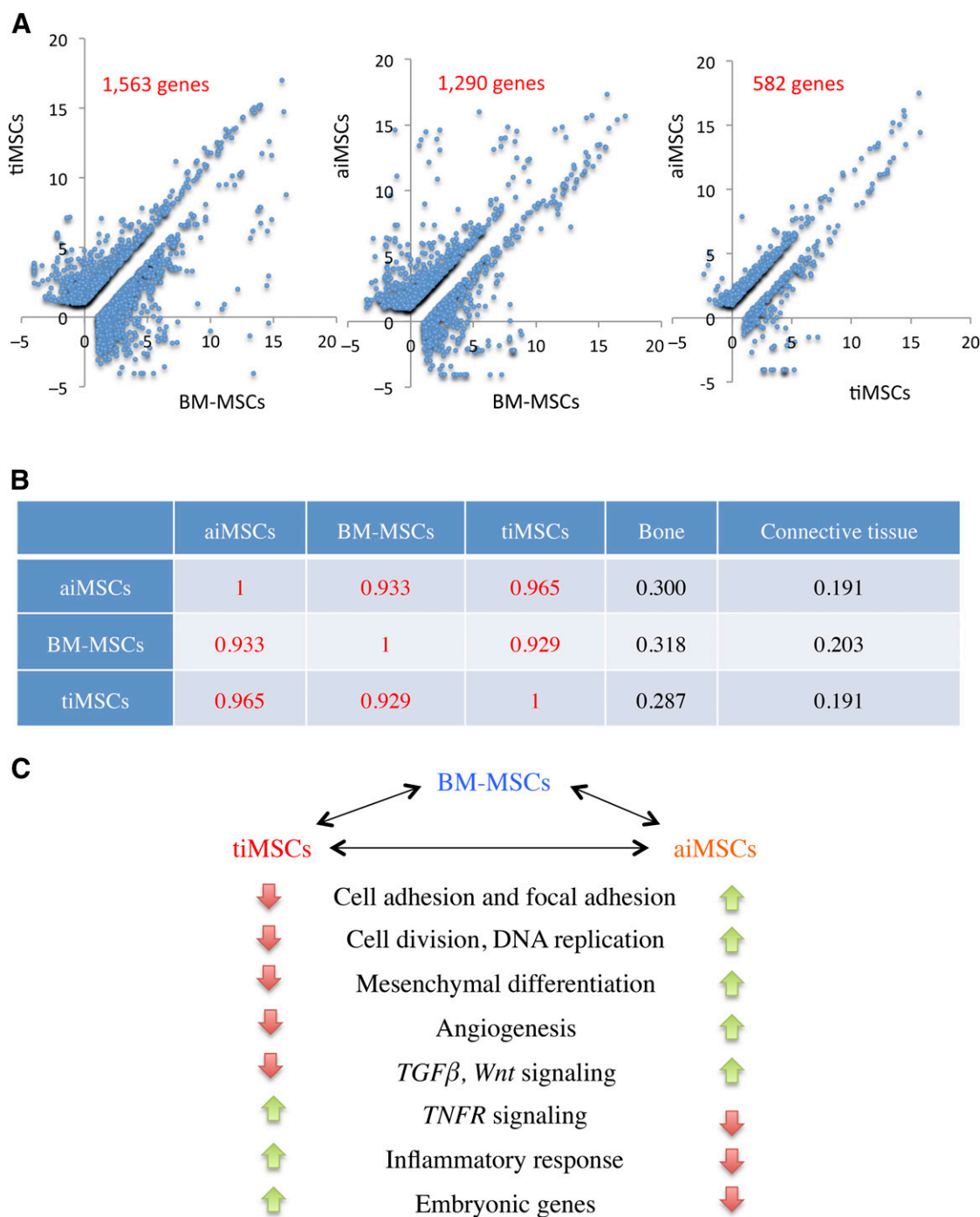
Figure 2. Transcriptomic comparison between iMSCs and BM-MSCs. **(A):** Overview of down- and upregulated genes in each cell type after thresholding ($p < .001$). **(B):** Comparison of the three cell types' transcriptomes to each other and to other cell lines based on information in available databases. Values represent the pairwise global correlation coefficient between cell lines. No correlation was found with other unlisted cell lines. **(C):** Summary of a gene ontology analysis in which both types of iMSCs were compared with BM-MSCs. Abbreviations: aiMSC, attached iMSC; BM-MSC, bone marrow-derived MSC; iMSC, iPSC-derived MSC; MSC, mesenchymal stem cell; tiMSC, transferred iMSC.

In Vivo Ectopic Bone Formation

Comparing in vivo ectopic bone formation from the three cell types overexpressing *BMP6*, we were surprised to find that injection of tiMSCs produced no or very little bone formation, whereas injection of aiMSCs produced substantial bone formation, similar to that found after injection of BM-MSCs (Fig. 5A). Quantitative μCT analysis revealed that bone volume of the ectopic bone induced by BM-MSCs was higher than that induced by tiMSCs ($p < .05$). No differences were found between the use of BM-MSCs and aiMSCs. Bone mineral density was similar after injection of all three cell types. Interestingly, the structural parameters of the ectopic bone showed that aiMSCs induced the formation of bone tissue of significantly higher trabecular thickness and connectivity density compared with BM-MSCs, but no
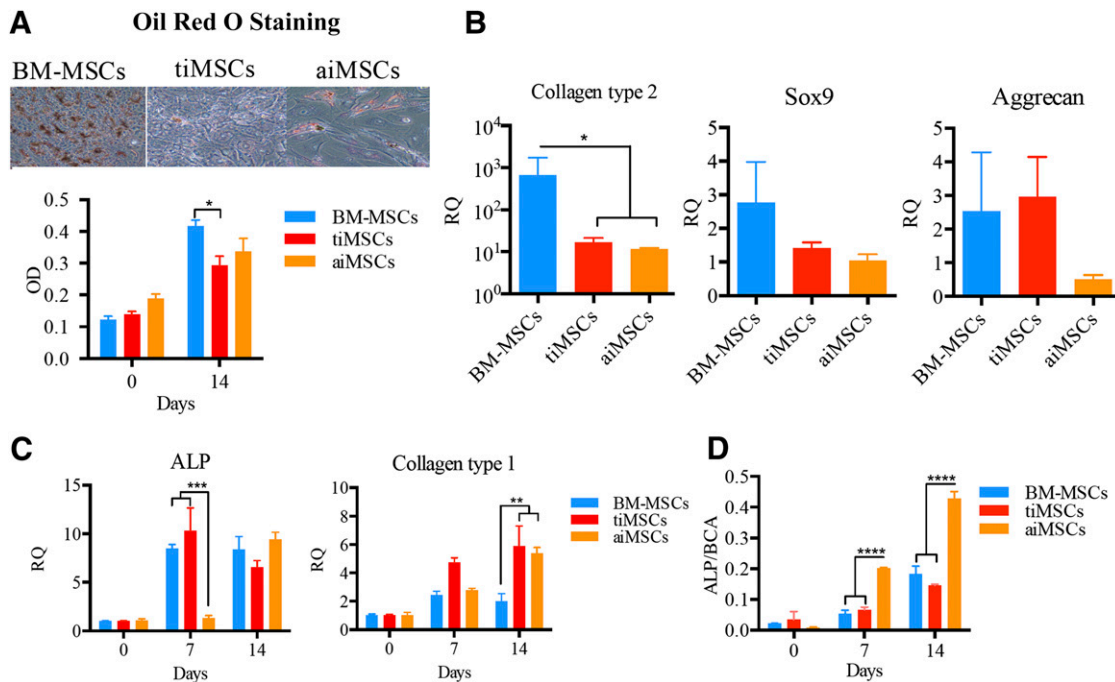
Figure 3. Differentiation potentials of iMSCs in vitro. **(A):** Supplement-induced adipogenic differentiation of BM-MSCs, tiMSCs, and aiMSCs was evaluated using Oil Red O staining and quantitative analysis. **(B):** Supplement-induced chondrogenic differentiation of BM-MSCs, tiMSCs, and aiMSCs in Transwells was evaluated by determining gene expression of *Collagen type II*, *Sox9*, and *Aggrecan* on day 21 postinduction. **(C):** Supplement-induced osteogenic differentiation of BM-MSCs, tiMSCs, and aiMSCs was evaluated by determining gene expression of ALP and collagen type 1, and by performing a quantitative ALP assay **(D)**. Results are presented as means ± SE. *, $p \leq .05$; **, $p \leq .01$; ***, $p \leq .001$; ****, $p \leq .0001$. Abbreviations: aiMSC, attached iMSC; ALP, alkaline phosphatase; BM-MSC, bone marrow-derived MSC; iMSC, iPSC-derived MSC; MSC, mesenchymal stem cell; OD, optical density; tiMSC, transferred iMSC.
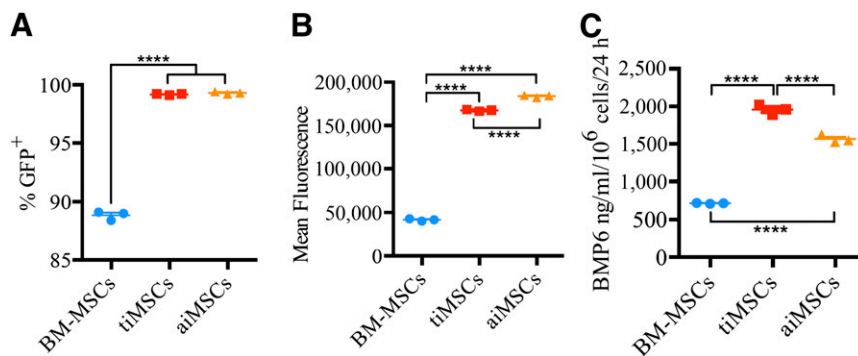
Figure 4. Efficiency of transfection of iMSCs using the reporter gene *GFP* and the therapeutic gene *BMP6*. BM-MSCs, tiMSCs and aiMSCs were transfected with a plasmid encoding for *GFP*. Flow cytometry was used to determine the percentage of *GFP*-expressing cells **(A)** and the mean fluorescence intensity **(B)**. **(C):** BM-MSCs, tiMSCs, and aiMSCs were transfected with a plasmid encoding for *BMP6*. ELISA was used to quantify the amount of BMP6 protein secreted into the media. Results are presented as means ± SE. ****, $p \leq .0001$ ($n = 3$). Abbreviations: aiMSC, attached iMSC; BM-MSC, bone marrow-derived MSC; BMD, bone mineral density; BMP, bone morphogenetic protein; BV, bone volume; ELISA, enzyme-linked immunosorbent assay; iMSC, iPSC-derived MSC; MSC, mesenchymal stem cell; tiMSC, transferred iMSC.

significant differences were found compared with tiMSCs (Fig. 5B). Histologic analysis confirmed ectopic bone formation following implantation of *BMP6*-overexpressing aiMSCs and BM-MSCs and very little bone formation when tiMSCs were implanted. Most tiMSCs seemed to preserve their fibroblastic morphology, and the majority of these cells did not differentiate in vivo (Fig. 5C).

Radial Defect Regeneration Using iMSCs

Nonunion radial defects were created in immunocompromised mice as previously reported [63, 67]. The cells were nucleofected

with *BMP6*, as described earlier, and implanted into the defects on DuraGen sponges. The regeneration process was monitored by performing μCT in vivo for up to 8 weeks, and the results show that the defect was completely regenerated by week 8 after the surgery in the MSC-BMP6 treated groups, but not in the control group (Fig. 6A, 6B). Surprisingly, the group treated with tiMSCs had significantly higher bone volume in the region of the radial defects, not only compared with untreated controls, but also with aiMSCs and BM-MSCs on weeks 4 and 8 postsurgery (Fig. 6B). When we checked the contribution of the implanted
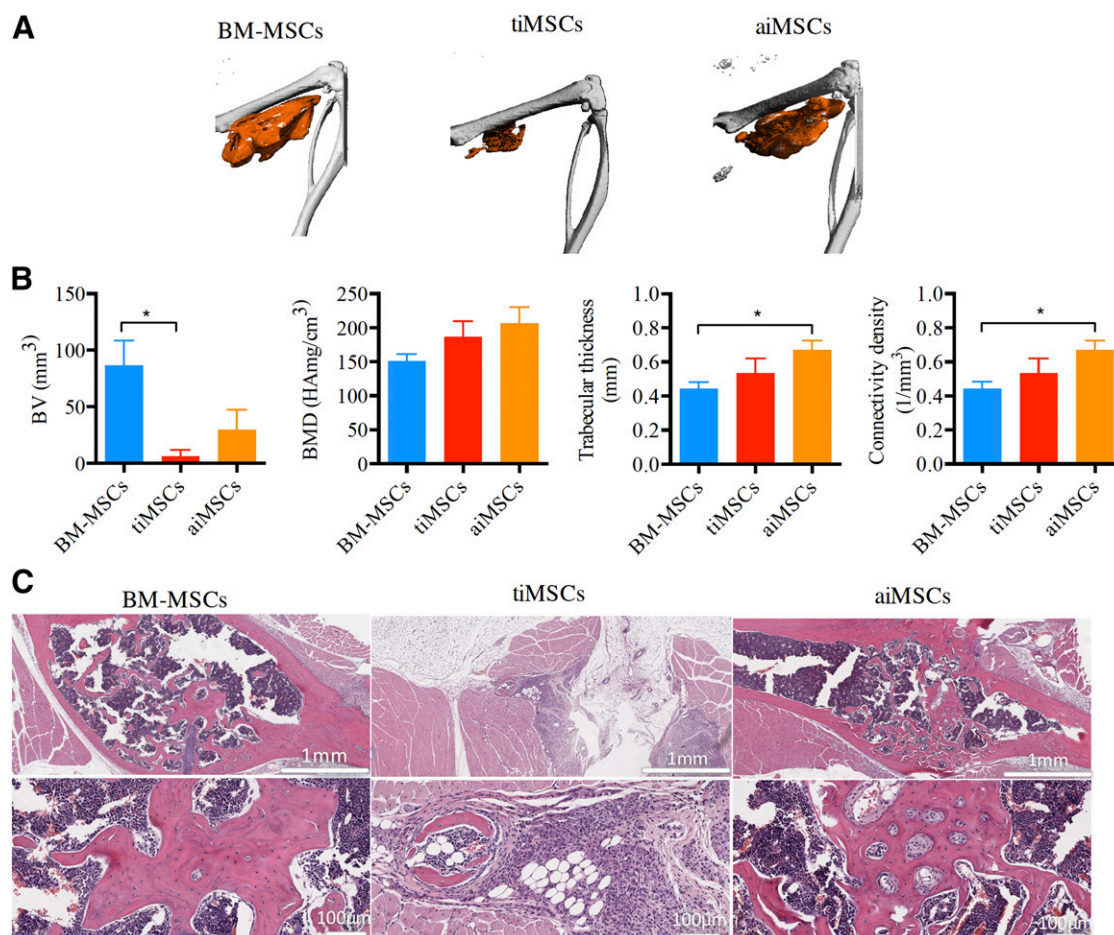
Figure 5. iMSCs induce ectopic bone formation following overexpression of *BMP6*. Thigh muscles of immunodeficient mice were injected with *BMP6*-transfected aiMSCs, tiMSCs, or BM-MSCs. Four weeks later, ectopic bone formation was evaluated using μCT. **(A):** A representative thigh and leg μCT reconstruction (new bone formation highlighted in orange) is shown for each treatment group. **(B):** Bone volume, bone mineral density, connectivity density, and trabecular thickness were calculated based on μCT data for each treatment groups. **(C):** Hematoxylin & eosin sections of the ectopic bone at two magnifications were evaluated for each treatment group. Results are presented as means $\pm$ SE. $*$, $p \leq .05$ (n = 5). Abbreviations: aiMSC, attached iMSC; BM-MSC, bone marrow-derived MSC; BV, bone volume; iMSC, iPSC-derived MSC; μCT, micro-computed tomography; MSC, mesenchymal stem cell; tiMSC, transferred iMSC; TV, trabecular volume.

cells to the in vivo bone formation and the regeneration process, we identified Dil-prelabeled BM-MSCs and iMSCs in the defect areas (Fig. 7B). Additionally, when examining tissue sections stained for the osteogenic markers BSP and OC, we could identify an overlay between Dil-stained cells and osteogenic marker (BSP and OC) stained cells (Fig. 7B) in all groups, besides the untreated control.

DISCUSSION

The therapeutic potential of MSCs has been known for several decades and demonstrated multiple times for a broad variety of tissues, organs, and conditions. MSCs have been successfully isolated from multiple tissues, and their immunoprivileged status makes them attractive as an autologous therapeutic agent. Nevertheless, their expansion capacity is limited, and their characteristics tend to change in vitro, which may divert them from their primary MSC phenotype and behavior. Additionally, the availability of MSCs is limited as a result of the comorbidity and complications associated with MSC harvest from adipose tissue or bone marrow. For these reasons, iPSC-derived MSCs are attractive candidates for stem cell therapy, because they

have the unlimited capacity of expansion at the iPSC stage, and the iMSCs shown here fulfill the minimal criteria to be defined as MSCs [68].

Several methods were recently developed to differentiate iPSCs into MSCs [69–75]. The functionality of these cells has been demonstrated in the cardiovascular system [72], as immunomodulatory cells [75], and as periodontal tissue-regenerating cells [70]. The method described here was based on a study by Li et al. [37] that used murine iPSCs as the progenitors of osteogenic MSCs. Noticing the formation of two different cell populations when applying the aforementioned approach to human iPSCs, we decided to investigate the differences between these two populations in their phenotypes, differentiation, and therapeutic potential.

We found that both types of iMSCs are highly proliferative but not tumorigenic. Both acquired MSC surface markers by 4–6 weeks postdifferentiation. Our results showed that passage 3–4 iMSCs, which were used for the in vivo studies, showed higher proliferation rates than BM-MSCs, similar surface marker gene expression, and lower colony-forming capability in soft agar, suggesting lower tumorigenic capabilities. In
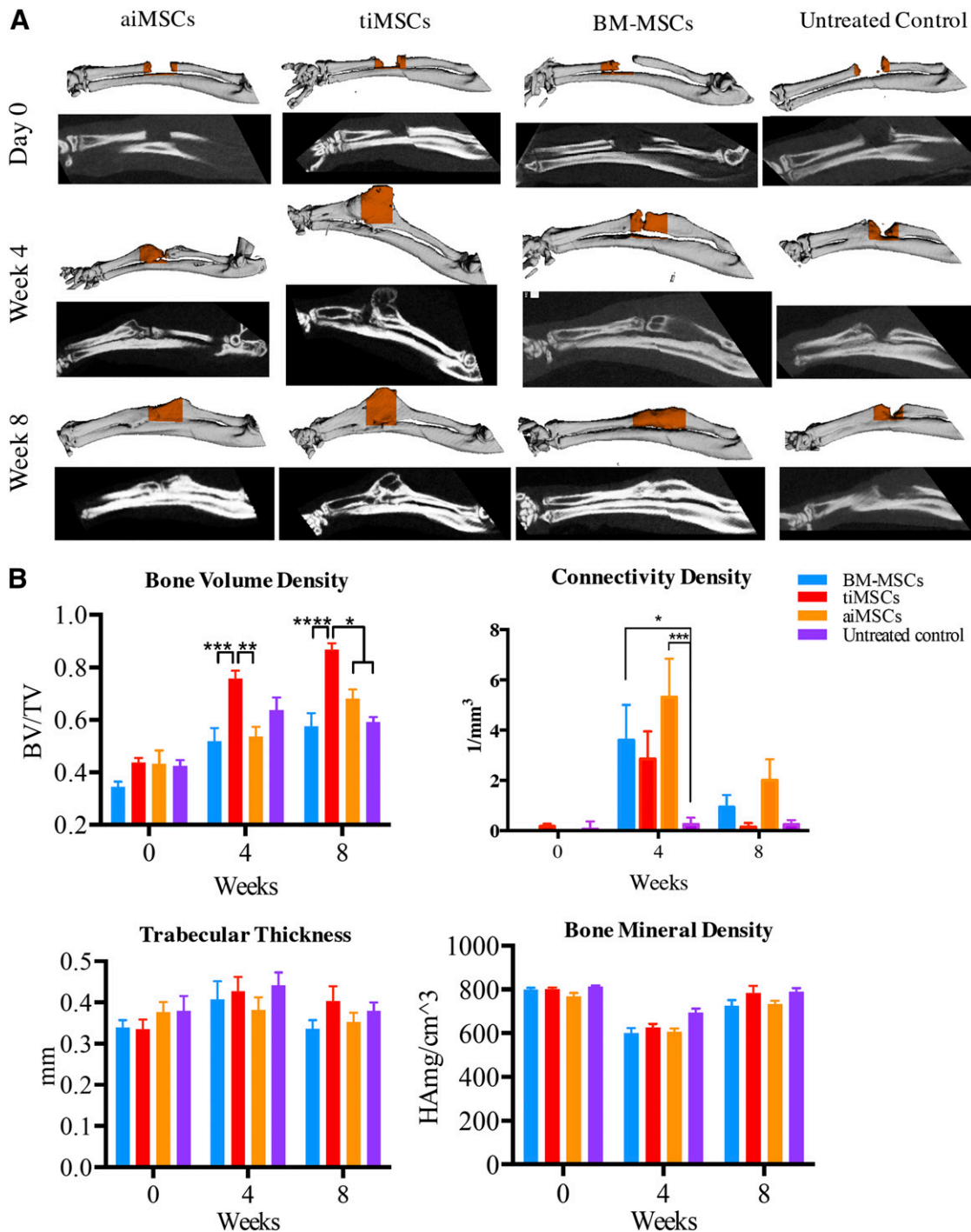
Figure 6. iMSCs regenerate bone in radial defects following overexpression of *BMP6*: longitudinal μCT imaging. Radial defects were created in immunocompromised mice and treated with BM-MSCs, aiMSCs, or tiMSCs overexpressing BMP6 or untreated controls. The regeneration process was imaged and analyzed using μCT. **(A):** Representative forearm μCT reconstruction (top, new bone formation highlighted in orange) and a mid-fracture μCT two-dimensional section (bottom) are shown for each treatment group at day 0, week 4, and week 8. **(B):** Bone volume density, bone mineral density, connectivity density, and trabecular thickness were calculated for each treatment group at day 0, week 4, and week 8. Results are presented as means $\pm$ SE. $*$, $p \leq .05$; $**$, $p \leq .01$; $***$, $p \leq .001$; $****$, $p \leq .0001$. Abbreviations: aiMSC, attached iMSC; BM-MSC, bone marrow-derived MSC; iMSC, iPSC-derived MSC; μCT, micro-computed tomography; MSC, mesenchymal stem cell; tiMSC, transferred iMSC.

spite of being more permissive for therapeutic gene transfection, thus probably generating more BMP6 in vivo, both were less efficient in inducing ectopic bone formation in vivo than BM-MSCs. Importantly, *BMP6*-overexpressing tiMSCs were significantly more efficient in regenerating a segmental bone

defect, inducing higher bone formation volumes than all other groups.

These exciting results suggest that tiMSCs are highly suitable to become an autologous gene-modified stem cell-based therapy. They could be produced for an individual patient in theoretically
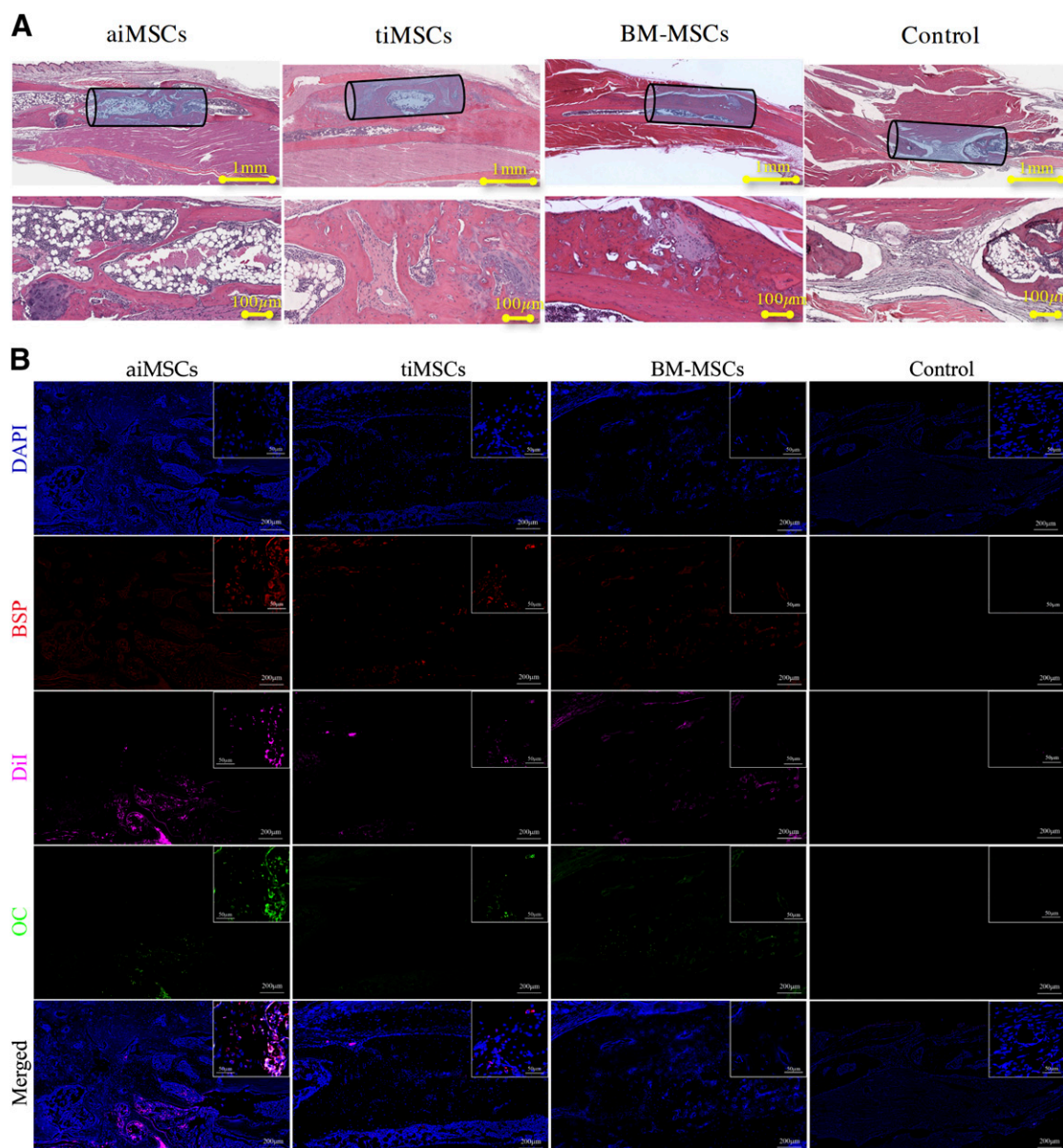
Figure 7. iMSCs differentiate in an orthotopic site and contribute to radial defect regeneration. Forelimbs were harvested at week 8 after surgery and subjected to histologic and immunofluorescence analyses. **(A):** Standard hematoxylin & eosin staining and imaging with a light microscope were done. Two magnifications are shown for each treatment group of a representative sample. The approximate location of bone void is marked by a cylinder. **(B):** Slides were immunostained for the osteogenic markers BSP and OC and counterstained with DAPI. Slides were then imaged using confocal microscopy for DAPI, DiI-labeled cells, OC, and BSP. A representative panel for each treatment group includes four single-channel images, each with a magnification inset and a merged image with a magnification inset. Abbreviations: BSP, bone sialoprotein; DAPI, 4′,6-diamidino-2-phenylindole dihydrochloride; iMSC, iPSC-derived MSC; MSC, mesenchymal stem cell; OC, osteocalcin.

limitless quantities without the comorbidities and complications associated with autologous MSC harvest. They may then be efficiently engineered to overexpress a therapeutic gene and locally administered to rapidly regenerate missing bone with the added benefit of reduced risk for ectopic bone formation compared with BM-MSCs, which are already considered safe.

Although they are very similar in many aspects, the striking difference between aiMSCs and tiMSCs in promoting bone regeneration may be attributed to a number of differences described in this study. First we should consider the original phenotypic difference that set tiMSCs apart from aiMSCs. We believe that aiMSCs, which grow out of EBs during an earlier stage, acquire more of a stem cell phenotype, whereas tiMSCs, which grow out of EBs at a later stage, acquire a more differentiated phenotype that better supports their further differentiation toward osteoblasts and regeneration of the defect but does not allow them to induce bone formation, even when triggered by BMPs, unless additional triggers are released in the orthotopic site of bone fracture. This theory is also supported by the transcriptomic study that found significant differences in mesenchymal stem cell-related genes, cell division, and focal adhesion.

Additional differences include the higher average doubling rate in early-passage tiMSCs are shown to have. For example, tiMSCs' doubling rate was twice as high as that of aiMSCs' at passage 2, albeit not significantly ($p > .05$). This difference may have played a role in promoting fracture healing because the implanted cells were at passage 3 and thus presumably were more proliferative than aiMSCs of the same passage. tiMSCs where significantly more prone to undergo early osteogenic differentiation based on ALP and collagen type 1 expression on day 7 ($p < .0001$) (Fig. 3B). Finally, tiMSCs secreted significantly more BMP6 compared with aiMSCs ($p < .0001$) (Fig. 3C). Taking these results altogether, it appears that tiMSCs could have an advantage over aiMSCs in promoting early bone regeneration because they proliferate more rapidly, express higher levels of osteogenic genes early on, and express a higher level of BMP6. All of the above would be highly desirable for many bone regeneration applications, suggesting this therapeutic approach should be further tested in additional bone loss models. On the other hand, aiMSCs might be useful in applications that require the properties of MSCs that are additional to bone formation. For example, future studies may explore their effect on avascular necrosis, in which angiogenesis plays a pivotal role in tissue regeneration. Additionally, their anti-inflammatory properties, as evident from the transcriptomic analysis (Fig. 2) and unlimited availability of autologous cells, might be an advantage in therapies in which MSCs are used as treatment and prevention of graft-versus-host disease [76].

The use of BMPs for bone regeneration is widely accepted in the literature; however, lately concerns were raised with regard to their possible tumorigenic effect because of their role in inducing angiogenesis [77]. On the other hand, BMPs were found to play pivotal roles in stem cell homeostasis and differentiation [78]. There is some evidence that BMP-2 promotes several types of cancer including pancreatic and breast cancer [79]; on the other hand, overexpression of BMP-6 was shown to reduce melanoma by inducing apoptosis of oncogenically transformed keratinocytes and also downregulating transcription factors of the AP-1 family, which are critical oncogenic factors in this cancer model [80]. BMPs act as protumorigenic or antitumorigenic agents, depending on the cancer type [78]; however, there is no evidence that nonviral overexpression of BMP6 can induce tumorigenesis. Additionally, our data show that the very short-term overexpression is sufficient to induce osteogenic differentiation, so no long-term hazards are expected.

AUTHOR CONTRIBUTIONS

D. Sheyn: conception and design, collection and/or assembly of data, data analysis and interpretation, manuscript writing; S.B.-D., M.B., and W.T.: collection and/or assembly of data, data analysis and interpretation; G.S.: collection and/or assembly of data, data analysis and interpretation, manuscript writing; S.D.-M. and X.D.: collection and/or assembly of data; L.O. and A.S.: provision of study material; D. Sareen: provision of study material, manuscript writing; G.P., conception and design, data analysis and interpretation; Z.L.: data analysis and interpretation, statistical analysis; D.G.: conception and design, final approval of manuscript; Z.G.: conception and design, data analysis and interpretation, manuscript writing, final approval of manuscript.

DISCLOSURE OF POTENTIAL CONFLICTS OF INTEREST

The authors indicated no potential conflicts of interest.

REFERENCES

1 Cortés F, Deschaseaux F, Uchida N et al. HCA, an immunoglobulin-like adhesion molecule present on the earliest human hematopoietic precursor cells, is also expressed by stromal cells in blood-forming tissues. Blood 1999;93:826–837.

2 Marshall CJ, Moore RL, Thorogood P et al. Detailed characterization of the human aorta-gonad-mesonephros region reveals morphological polarity resembling a hematopoietic stromal layer. Dev Dyn 1999;215:139–147.

3 Campagnoli C, Roberts IA, Kumar S et al. Identification of mesenchymal stem/progenitor cells in human first-trimester fetal blood, liver, and bone marrow. Blood 2001;98:2396–2402.

4 Zuk PA, Zhu M, Ashjian P et al. Human adipose tissue is a source of multipotent stem cells. Mol Biol Cell 2002;13:4279–4295.

5 Bianco P, Riminucci M, Gronthos S et al. Bone marrow stromal stem cells: Nature, biology, and potential applications. STEM CELLS 2001;19:180–192.

6 Krampera M, Pizzolo G, Aprili G et al. Mesenchymal stem cells for bone, cartilage, tendon and skeletal muscle repair. Bone 2006;39:678–683.

7 Turgeman G, Pittman DD, Müller R et al. Engineered human mesenchymal stem cells: A novel platform for skeletal cell mediated gene therapy. J Gene Med 2001;3:240–251.

8 Sheyn D, Kallai I, Tawackoli W et al. Gene-modified adult stem cells regenerate vertebral bone defect in a rat model. Mol Pharm 2011;8:1592–1601.

9 Sheyn D, Kimelman-Bleich N, Pelled G et al. Ultrasound-based nonviral gene delivery induces bone formation in vivo. Gene Ther 2008;15:257–266.

10 Aslan H, Zilberman Y, Kandel L et al. Osteogenic differentiation of noncultured immunoisolated bone marrow-derived CD105+ cells. STEM CELLS 2006;24:1728–1737.

11 Kimelman N, Pelled G, Helm GA et al. Review: Gene- and stem cell-based therapeutics for bone regeneration and repair. Tissue Eng 2007;13:1135–1150.

12 Sun Y, Li W, Lu Z et al. Rescuing replication and osteogenesis of aged mesenchymal stem cells by exposure to a young extracellular matrix. FASEB J 2011;25:1474–1485.

13 Duscher D, Rennert RC, Januszyk M et al. Aging disrupts cell subpopulation dynamics and diminishes the function of mesenchymal stem cells. Sci Rep 2014;4:7144.

14 Beane OS, Fonseca VC, Cooper LL et al. Impact of aging on the regenerative properties of bone marrow-, muscle-, and adipose-derived mesenchymal stem/stromal cells. PLoS One 2014;9:e115963.

15 de Girolamo L, Lopa S, Arrigoni E et al. Human adipose-derived stem cells isolated from young and elderly women: Their differentiation potential and scaffold interaction during in vitro osteoblastic differentiation. Cytotherapy 2009;11:793–803.

16 Yukata K, Xie C, Li TF et al. Aging periosteal progenitor cells have reduced regenerative responsiveness to bone injury and to the anabolic actions of PTH 1-34 treatment. Bone 2014;62:79–89.

17 Lavasani M, Robinson AR, Lu A et al. Muscle-derived stem/progenitor cell dysfunction limits healthspan and lifespan in a murine progeria model. Nat Commun 2012;3:608.

18 Takahashi K, Yamanaka S. Induction of pluripotent stem cells from mouse embryonic and adult fibroblast cultures by defined factors. Cell 2006;126:663–676.

19 Pringle S, De Bari C, Dell'Accio F et al. Mesenchymal differentiation propensity of a human embryonic stem cell line. Cell Prolif 2011;44:120–127.

20 Laurila JP, Laatikainen L, Castellone MD et al. Human embryonic stem cell-derived mesenchymal stromal cell transplantation in a rat hind limb injury model. Cytotherapy 2009;11: 726–737.

21 Swijnenburg RJ, Tanaka M, Vogel H et al. Embryonic stem cell immunogenicity increases upon differentiation after transplantation into ischemic myocardium. Circulation 2005;112(suppl): I166–I172.

22 Sugarman J. Human stem cell ethics: Beyond the embryo. Cell Stem Cell 2008;2: 529–533.

23 Taura D, Noguchi M, Sone M et al. Adipogenic differentiation of human induced pluripotent stem cells: Comparison with that of human embryonic stem cells. FEBS Lett 2009;583: 1029–1033.

24 Mizuno Y, Chang H, Umeda K et al. Generation of skeletal muscle stem/progenitor cells from murine induced pluripotent stem cells. FASEB J 2010;24:2245–2253.

25 Kazuki Y, Hiratsuka M, Takiguchi M et al. Complete genetic correction of iPS cells from Duchenne muscular dystrophy. Mol Ther 2010; 18:386–393.

26 Lian Q, Zhang Y, Zhang J et al. Functional mesenchymal stem cells derived from human induced pluripotent stem cells attenuate limb ischemia in mice. Circulation 2010;121:1113–1123.

27 Song H, Yoon C, Kattman SJ et al. Interrogating functional integration between injected pluripotent stem cell-derived cells and surrogate cardiac tissue. Proc Natl Acad Sci USA 2010;107:3329–3334.

28 Sheyn D, Mizrahi O, Benjamin S et al. Genetically modified cells in regenerative medicine and tissue engineering. Adv Drug Deliv Rev 2010;62:683–698.

29 Levi B, Hyun JS, Montoro DT et al. In vivo directed differentiation of pluripotent stem cells for skeletal regeneration. Proc Natl Acad Sci USA 2012;109:20379–20384.

30 Knoepfler PS. Deconstructing stem cell tumorigenicity: A roadmap to safe regenerative medicine. STEM CELLS 2009;27:1050–1056.

31 Flavell RA, Sanjabi S, Wrzesinski SH et al. The polarization of immune cells in the tumour environment by TGFbeta. Nat Rev Immunol 2010;10:554–567.

32 Itoh F, Watabe T, Miyazono K. Roles of TGF-β family signals in the fate determination of pluripotent stem cells. Semin Cell Dev Biol 2014;32:98–106.

33 Li Z, Yang CS, Nakashima K et al. Small RNA-mediated regulation of iPS cell generation. EMBO J 2011;30:823–834.

34 Yamasaki S, Taguchi Y, Shimamoto A et al. Generation of human induced pluripotent stem (Ips) cells in serum- and feeder-free defined culture and TGF-Β1 regulation of pluripotency. PLoS One 2014;9:e87151.

35 Chen YS, Pelekanos RA, Ellis RL et al. Small molecule mesengenic induction of human induced pluripotent stem cells to generate mesenchymal stem/stromal cells. STEM CELLS TRANSLATIONAL MEDICINE 2012;1:83–95.

36 Kato H, Ochiai-Shino H, Onodera S et al. Promoting effect of 1,25(OH)2 vitamin D3 in osteogenic differentiation from induced pluripotent stem cells to osteocyte-like cells. Open Biol 2015;5:140201.

37 Li F, Bronson S, Niyibizi C. Derivation of murine induced pluripotent stem cells (iPS) and assessment of their differentiation toward osteogenic lineage. J Cell Biochem 2010;109: 643–652.

38 Gautschi OP, Frey SP, Zellweger R. Bone morphogenetic proteins in clinical applications. ANZ J Surg 2007;77:626–631.

39 Kang Q, Sun MH, Cheng H et al. Characterization of the distinct orthotopic bone-forming activity of 14 BMPs using recombinant adenovirus-mediated gene delivery. Gene Ther 2004;11:1312–1320.

40 Kimelman-Bleich N, Pelled G, Zilberman Y et al. Targeted gene-and-host progenitor cell therapy for nonunion bone fracture repair. Mol Ther 2011;19:53–59.

41 Sheyn D, Rüthemann M, Mizrahi O et al. Genetically modified mesenchymal stem cells induce mechanically stable posterior spine fusion. Tissue Eng Part A 2010;16:3679–3686.

42 Paul S, Lee JC, Yeh LC. A comparative study on BMP-induced osteoclastogenesis and osteoblastogenesis in primary cultures of adult rat bone marrow cells. Growth Factors 2009;27: 121–131.

43 Luu HH, Song WX, Luo X et al. Distinct roles of bone morphogenetic proteins in osteogenic differentiation of mesenchymal stem cells. J Orthop Res 2007;25:665–677.

44 Zachos TA, Shields KM, Bertone AL. Gene-mediated osteogenic differentiation of stem cells by bone morphogenetic proteins-2 or -6. J Orthop Res 2006;24:1279–1291.

45 Carpenter RS, Goodrich LR, Frisbie DD et al. Osteoblastic differentiation of human and equine adult bone marrow-derived mesenchymal stem cells with BMP-2 or BMP-7 homodimer genetic modification is compared to BMP-2/7 heterodimer genetic modification in the presence and absence of dexamethasone. J Orthop Res 2010;28:1330–1337.

46 Li JZ, Li H, Sasaki T et al. Osteogenic potential of five different recombinant human bone morphogenetic protein adenoviral vectors in the rat. Gene Ther 2003;10:1735–1743.

47 Cheng H, Jiang W, Phillips FM et al. Osteogenic activity of the fourteen types of human bone morphogenetic proteins (BMPs). J Bone Joint Surg Am 2003;85-A:1544–1552.

48 Aslan H, Zilberman Y, Arbeli V et al. Nucleofection-based ex vivo nonviral gene delivery to human stem cells as a platform for tissue regeneration. Tissue Eng 2006;12: 877–889.

49 Hasharoni A, Zilberman Y, Turgeman G et al. Murine spinal fusion induced by engineered mesenchymal stem cells that conditionally express bone morphogenetic protein-2. J Neurosurg Spine 2005;3:47–52.

50 Moutsatsos IK, Turgeman G, Zhou S et al. Exogenously regulated stem cell-mediated gene therapy for bone regeneration. Mol Ther 2001;3:449–461.

51 Mizrahi O, Sheyn D, Tawackoli W et al. BMP-6 is more efficient in bone formation than BMP-2 when overexpressed in mesenchymal stem cells. Gene Ther 2013;20: 370–377.

52 Sheyn D, Pelled G, Zilberman Y et al. Non-virally engineered porcine adipose tissue-derived stem cells: Use in posterior spinal fusion. STEM CELLS 2008;26:1056–1064.

53 Okita K, Matsumura Y, Sato Y et al. A more efficient method to generate integration-free human iPS cells. Nat Methods 2011;8:409–412.

54 Sareen D, O'Rourke JG, Meera P et al. Targeting RNA foci in iPSC-derived motor neurons from ALS patients with a C9ORF72 repeat expansion. Sci Transl Med 2013;5: 208ra149.

55 Sareen D, Gowing G, Sahabian A et al. Human induced pluripotent stem cells are a novel source of neural progenitor cells (iNPCs) that migrate and integrate in the rodent spinal cord. J Comp Neurol 2014;522:2707–2728.

56 Barrett R, Ornelas L, Yeager N et al. Reliable generation of induced pluripotent stem cells from human lymphoblastoid cell lines. STEM CELLS TRANSLATIONAL MEDICINE 2014;3: 1429–1434.

57 Kuroda T, Yasuda S, Kusakawa S et al. Highly sensitive in vitro methods for detection of residual undifferentiated cells in retinal pigment epithelial cells derived from human iPS cells. PLoS One 2012;7:e37342.

58 Huang W, Sherman BT, Lempicki RA. Systematic and integrative analysis of large gene lists using DAVID bioinformatics resources. Nat Protoc 2009;4:44–57.

59 Mizrahi O, Sheyn D, Tawackoli W et al. Nucleus pulposus degeneration alters properties of resident progenitor cells. Spine J 2013; 13:803–814.

60 Sheyn D, Pelled G, Tawackoli W et al. Transient overexpression of Pparγ2 and C/ebpα in mesenchymal stem cells induces brown adipose tissue formation. Regen Med 2013;8:295–308.

61 Risbud MV, Albert TJ, Guttapalli A et al. Differentiation of mesenchymal stem cells towards a nucleus pulposus-like phenotype in vitro: Implications for cell-based transplantation therapy. Spine 2004;29:2627–2632.

62 Risbud MV, Guttapalli A, Tsai TT et al. Evidence for skeletal progenitor cells in the degenerate human intervertebral disc. Spine 2007;32: 2537–2544.

63 Tai K, Pelled G, Sheyn D et al. Nanobiomechanics of repair bone regenerated by genetically modified mesenchymal stem cells. Tissue Eng Part A 2008;14:1709–1720.

64 Kallai I, Mizrahi O, Tawackoli W et al. Microcomputed tomography-based structural analysis of various bone tissue regeneration models. Nat Protoc 2011;6:105–110.

65 Müller R, Rüegsegger P. Micro-tomographic imaging for the nondestructive evaluation of trabecular bone architecture. Stud Health Technol Inform 1997;40:61–79.

66 Hildebrand T, Laib A, Müller R et al. Direct three-dimensional morphometric analysis of human cancellous bone: microstructural data from spine, femur, iliac crest, and calcaneus. J Bone Miner Res 1999;14:1167–1174.

67 Kimelman-Bleich N, Pelled G, Sheyn D et al. The use of a synthetic oxygen carrier-enriched hydrogel to enhance mesenchymal stem cell-based bone formation in vivo. Biomaterials 2009;30:4639–4648.

68 Dominici M, Le Blanc K, Mueller I et al. Minimal criteria for defining multipotent mesenchymal stromal cells. The International Society for Cellular Therapy position statement. Cytotherapy 2006;8:315–317.

69 Yang H, Aprecio RM, Zhou X et al. Therapeutic effect of TSG-6 engineered iPSC-derived MSCs on experimental periodontitis in rats: A pilot study. PLoS One 2014;9: e100285.

70 Frobel J, Hemeda H, Lenz M et al. Epigenetic rejuvenation of mesenchymal stromal cells derived from induced pluripotent stem cells. Stem Cell Rep 2014;3:414–422.

71 Hynes K, Menicanin D, Mrozik K et al. Generation of functional mesenchymal stem cells from different induced pluripotent stem cell lines. Stem Cells Dev 2014;23:1084–1096.

72 Buccini S, Haider KH, Ahmed RP et al. Cardiac progenitors derived from reprogrammed mesenchymal stem cells contribute to angio-myogenic repair of the infarcted heart. Basic Res Cardiol 2012;107:301.

73 Liu Y, Goldberg AJ, Dennis JE et al. One-step derivation of mesenchymal stem cell (MSC)-like cells from human pluripotent stem cells on a fibrillar collagen coating. PLoS One 2012;7:e33225.

74 Villa-Diaz LG, Brown SE, Liu Y et al. Derivation of mesenchymal stem cells from human induced pluripotent stem cells cultured on synthetic substrates. STEM CELLS 2012;30: 1174–1181.

75 Giuliani M, Oudrhiri N, Noman ZM et al. Human mesenchymal stem cells derived from induced pluripotent stem cells down-regulate NK-cell cytolytic machinery. Blood 2011;118: 3254–3262.

76 von Dalowski F, Kramer M, Wermke M et al. Mesenchymal stromal cells for treatment of acute steroid-refractory GvHD: Clinical responses and long-term outcome. STEM CELLS 2016;34:357–366.

77 Ye L, Jiang WG. Bone morphogenetic proteins in tumour associated angiogenesis and implication in cancer therapies. Cancer Lett 2015 (Nov):27.

78 Davis H, Raja E, Miyazono K et al. Mechanisms of action of bone morphogenetic proteins in cancer. Cytokine Growth Factor Rev 2015;27:81–92.

79 Li CS, Tian H, Zou M et al. Secreted phosphoprotein 24 kD (Spp24) inhibits growth of human pancreatic cancer cells caused by BMP-2. Biochem Biophys Res Commun 2015;466: 167–172.

80 Wach S, Schirmacher P, Protschka M et al. Overexpression of bone morphogenetic protein-6 (BMP-6) in murine epidermis suppresses skin tumor formation by induction of apoptosis and downregulation of fos/jun family members. Oncogene 2001;20:7761–7769.

See www.StemCellsTM.com for supporting information available online.